Optical magnetism in core-satellite nanostructures excited by vector beams

John Parker[a,b], Stephen Gray[d], and Norbert F. Scherer[a,c,*]

[a]James Franck Institute, University of Chicago, Chicago, IL 60637 USA
[b]Department of Physics, University of Chicago, Chicago, IL 60637 USA
[c]Department of Chemistry, University of Chicago, Chicago, IL 60637 USA
[d]Center for Nanoscale Materials, Argonne National Laboratory, Chicago, IL 60439 USA

ABSTRACT

Core-satellite nanostructures are meta-atom candidates that have strong magnetic modes at optical frequencies and their characterization is important for developing them into metamaterials and metafluids. We utilize an electrodynamics-multipolar analysis (ED-MA) method to perform a detailed study of the electric and magnetic modes of a core-satellite nanostructure composed of silver nanoparticles decorated on a dielectric core. In addition to excitation with linearly polarized scalar beams, we utilize radially and azimuthally polarized cylindrical vector beams to selectively excite and enhance the electric and magneticmultipolar modes of the core-satellite nanostructure. The refractive index of the dielectric core is altered to better understand the role of retardation in the unique multipolar modes that arise from these vector beam excitations. A more complex Ag-core silica-shell nanostructure decorated with Ag-satellites is also introduced and is shown to diminish the role of magnetic modes and introduce new electric modes selectively excited by a radially polarized beam.

Keywords: optics, microscopy, metamaterials, vector beams

1. INTRODUCTION

Creating negative-index metamaterials requires both a negative permittivity and permeability at the same excitation frequencies.[1–4] Metamaterials and metafluids can potentially be built from suitable nanoscale structured "meta-atom" building blocks in a bottom-up fashion.[5–12] In order to obtain negative values for these effective medium parameters, the medium must be composed of meta-atoms with strong electric and magnetic resonances. It is thus important to be able to measure, characterize, and control the dipolar and higher-order multipolar resonances in nanoscale engineered materials for optimization. The introduction of vector beam sources can provide a further level of control and selectivity over the meta-atom's multipolar modes, providing new ways of characterizing nanoscale materials by simply changing the illumination.[13–16]

Previous theoretical and experimental studies of core-satellite nanostructures (a dielectric core decorated with metal nanoparticles on the core's surface) have identified a strong collective magnetic mode, making them a good meta-atom candidate.[5–12,15,16] Experimental work on small core-satellite nanostructures have identified a magnetic dipole mode using angular scattering techniques and applied a Maxwell-Garnett effective medium model approach to the bulk metafluid, showing that the effective bulk permeability could be tuned.[6] Vector beam sources have been shown to selectively excite and enhance multipolar modes of the core-satellite nanostructure.[15,16] In particular, azimuthally polarized beams have been shown to selectively excite and enhance the magnetic modes of the core-satellite nanostructure, making it a useful tool in the study of optical magnetism.

To understand the multipolar nature of the core-satellite nanostructure, we developed an electrodynamics-multipolar analysis (ED-MA) method[16] combined with the Finite-Difference Time-Domain (FDTD) method,[17] using a freely available software package.[18] We applied this rigorous ED-MA multipolar characterization method to dielectric core-Ag nanoparticle satellite structures under both scalar and vector beam illumination. Excitation with azimuthally polarized beams results in selective excitation of magnetic modes while radially polarized beams

*Corresponding author: nfschere@uchicago.edu

selectivity excite electric modes. The findings described in detail in this paper are in agreement with previous experiments[15] and simulations.[16]

To better understand the electric and magnetic properties of the core-satellite nanostructure, we vary properties of the core region. By varying the index of refraction of the dielectric core, we find that the role of retardation in these excitations can spectrally shift modes and cause a unique disappearance of the magnetic dipole mode. We also introduce a core-shell-satellite nanostructure (a core-satellite nanostructure with an Ag nanoparticle embedded in the silica core). A new electric mode selectively excited by the radially polarized beam is discovered, while the magnetic modes excited by azimuthally polarized light are diminished, i.e. the metal core expels the magnetic field.

2. METHODS

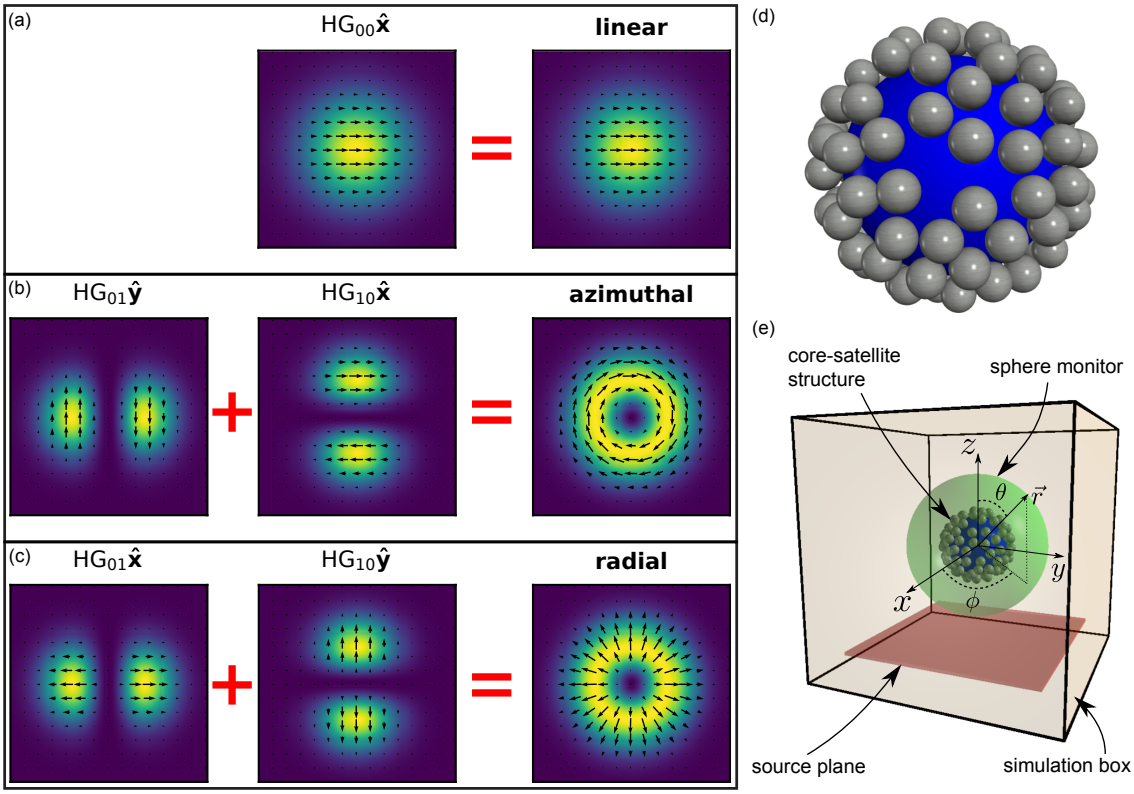

Figure 1. Simulation setup for the excitation of core-satellite nanostructures by vector beams with multipolar analysis. (a) The linearly polarized beam is composed of the x-polarized HG_{00} mode. (b) The azimuthally polarized beam is a combination of the y-polarized HG_{01} mode and the x-polarized HG_{10} mode. (c) The radially polarized beam is a combination of the x-polarized HG_{01} mode and the y-polarized HG_{10} mode. Arrows denote the electric field polarization. (d) A randomly packed silica-core Ag-nanoparticle core-satellite nanostructure with 104 Ag nanoparticles. (e) Simulation box that defines the coordinate system and shows the source plane, core-satellite nanostructure, and spherical monitor used for the multipolar analysis.

The core-satellite nanostructure considered here consists of a 250 nm diameter silica core and 104 silver nanoparticles (40 nm in diameter) randomly packed on the surface of the sphere (Figure 2(d)). All nanoparticles maintain a minimum surface-to-surface separation of 2 nm to prevent nanoparticle overlap. The silica core is treated as a dielectric with a constant index of refraction $n_{\text{core}} = 1.46$, and the surrounding medium is taken to be oil of index $n_{\text{oil}} = 1.51$. The silver nanoparticles are modeled with a Drude-Lorentz dispersive permittivity $\varepsilon_{\text{ag}}(\omega)$ model chosen to fit experimental data.[19,20] The algorithm used to randomly place nanoparticles on the surface of the core is described in greater detail in previous work.[16]

Finite-Difference Time-Domain (FDTD) simulations are performed using the freely available MEEP software package.[17,18] The core-satellite nanostructure is embedded in the FDTD grid using a sub-pixel smoothing algorithm.[21,22] All simulations use a 2 nm spatial resolution and a Courant factor of 0.5. A 40 nm thick perfectly matched layer (PML) boundary condition was employed to dissipate fields at the simulation box edges.

The radially and azimuthally polarized cylindrical vector beams are created from combinations of the lowest-order Hermite-Gaussian modes.[23,24] The electric field for the vector beams and the linearly polarized scalar beam are

$$\begin{aligned} \boldsymbol{E}_{\text{lin}} &= \text{HG}_{00}\hat{\boldsymbol{x}} \\ \boldsymbol{E}_{\text{azi}} &= \text{HG}_{01}\hat{\boldsymbol{y}} + \text{HG}_{10}\hat{\boldsymbol{x}} \\ \boldsymbol{E}_{\text{rad}} &= \text{HG}_{01}\hat{\boldsymbol{x}} + \text{HG}_{10}\hat{\boldsymbol{y}} \end{aligned} \tag{1}$$

These linear combinations are visually demonstrated in Figure 2(a-c). Each panel is an xy cross-section of the incident beam at the focal plane. In the FDTD simulation, the focal plane must be chosen outside of the core-satellite nanostructure and is thus chosen to be 50 nm from the nanoparticle surface to minimize the beam's divergence across the sample (red plane in Figure 2(e)) The coordinate system is defined in Figure 2(e). The x and y-axes span the source plane and the beams propagate along the $+z$-axis.

The ED-MA method has been detailed previously,[16] so only a summary is presented here for convenience. The electromagnetic fields are collected on the surface of a far-field sphere centered on the core-satellite nanostructure via a Near-to-Far-Field (NTFF) transformation[25] (green sphere in Figure 2(e)). The scattered electric field, $\boldsymbol{E}_{\text{scat}}(\omega, r, \theta, \phi)$, can be expanded into a complete set of basis functions, the vector spherical harmonics (VSHs)[26,27]

$$\boldsymbol{E}_{\text{scat}}(\omega, r, \theta, \phi) = \sum_{l=1}^{\infty} \sum_{m=-l}^{m=l} a_{lm}(\omega)\boldsymbol{N}_{lm} + b_{lm}(\omega)\boldsymbol{M}_{lm} \tag{2}$$

where $a_{lm}(\omega)$ and $b_{lm}(\omega)$ are the complex multipolar coefficients corresponding to the electric ($\boldsymbol{N}_{lm}$) and magnetic ($\boldsymbol{M}_{lm}$) modes, respectively, of order l and orientation m at frequency ω.

An equation for the multipolar coefficients $a_{lm}(\omega)$ and $b_{lm}(\omega)$ can be determined by using orthogonality relationships between the VSHs

$$\begin{aligned} a_{lm}(\omega) &= \oint_{\Omega} \boldsymbol{E}_{\text{scat}}(\omega, r = r_0, \theta, \phi) \cdot \boldsymbol{N}_{lm}(\omega, r = r_0, \theta, \phi)\, d\Omega \\ b_{lm}(\omega) &= \oint_{\Omega} \boldsymbol{E}_{\text{scat}}(\omega, r = r_0, \theta, \phi) \cdot \boldsymbol{M}_{lm}(\omega, r = r_0, \theta, \phi)\, d\Omega \end{aligned} \tag{3}$$

where r_0 is the radius of the spherical monitor and Ω is the far-field sphere surface. For each frequency ω of interest, Eq.(3) is used to numerically compute the multipolar scattering coefficients. To connect the multipolar coefficients to the scattering cross-section, we use the relation[26]

$$\sigma_{\text{scat}}(\omega) = k^2 \sum_{l=1}^{\infty} \sum_{m=-n}^{n} l(l+1)\left(|a_{lm}(\omega)|^2 + |b_{lm}(\omega)|^2\right) \tag{4}$$

where $k = 2\pi n_{\text{b}}/\lambda$, and $n_b = 1.51$. Each l term in the first sum provides the scattering cross-section contribution of the corresponding multipolar mode, where $l = 1$ is dipole, $l = 2$ is quadrupole, etc. A scattering efficiency is obtained by normalizing the scattering cross-section by the cross-sectional area of the core-satellite, $A = \pi(r_1 + 2r_2)^2 = \pi(125\,\text{nm} + 40\,\text{nm})^2 \approx 85.5\,\mu\text{m}^2$, where r_1 is the radius of the core and r_2 is the radius of the Ag nanoparticles.

3. SELECTIVE EXCITATION OF OPTICAL MODES BY CYLINDRICAL VECTOR BEAMS

An FDTD simulation using the ED-MA method was performed for the core-satellite nanostructure for linearly, azimuthally, and radially polarized excitation. The total scattering efficiencies are shown in Figure 2(a) on an

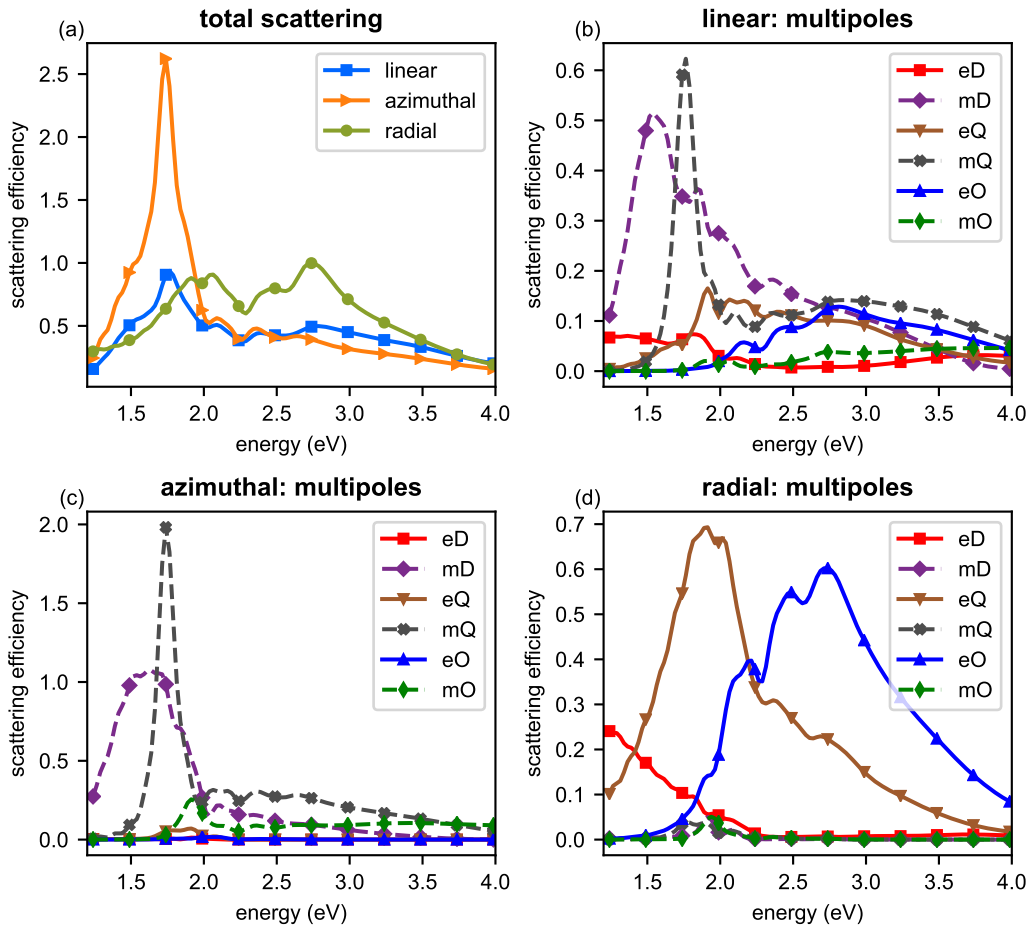

Figure 2. Selective excitation of multipolar modes in core-satellite nanostructures by vector beams. (a) Total scattering by linearly, azimuthally, and radially polarized beams. (b-d) Multipolar scattering for linearly, azimuthally, and radially polarized beams, respectively. The labels indicate the multipolar mode: e = electric, m = magnetic, D = dipole, Q = quadrupole, O = octupole (dashed lines = magnetic modes, solid lines = electric modes).

energy scale. The azimuthally polarized excitation shows a sharp peak at 1.8 eV. Radially polarized excitation exhibits multiple spectral features from 1.8 eV to 3.0 eV with the strongest peak at 2.8 eV. We can see that the beams excite different modes with different amplitudes, but further insight is not available from total scattering.

The multipolar scattering reveals more about the excitations created by different beams. The ED-MA method is used to compute both electric and magnetic modes of order $l = 1$ (dipole), $l = 2$ (quadrupole) and $l = 3$ (octupole). For linearly polarized excitation (Figure 2(b)), contributions are found from all 6 modes, with strong contributions from magnetic dipole and magnetic quadrupole modes in the energy range from 1.5 eV to 2.0 eV. The electric dipole and magnetic octupole are found to be the weakest modes.

For azimuthally polarized excitation (Figure 2(c)), contributions to the scattering from electric dipole, electric quadrupole, and electric octupole become negligible. Similar to the linearly polarized excitation, the magnetic octupole is also weak compared to the two remaining modes, the magnetic dipole and magnetic quadrupole modes. This result indicates that the azimuthally polarized beam selectively excites the magnetic modes of the core-satellite nanostructure. The magnetic dipole and magnetic quadrupole modes share a similar excitation energy and spectral shape to those excited by the linearly polarized beam. We note that the amplitude of these two modes excited by the azimuthally polarized beam has been enhanced by up to a factor of 4 (vs. linearly polarized excitation) and the relative amplitude between these two modes has changed.

For radially polarized excitation (Figure 2(d)), contributions to the scattering from magnetic dipole, magnetic quadrupole, and magnetic octupole modes become negligible. Similar to the linearly polarized excitation, the electric dipole is also weak compared to the two remaining modes, the electric quadrupole and electric octupole modes. This result indicates that the radially polarized beam selectively excites the electric modes of the core-satellite nanostructure. Similar to the relationship between the azimuthally polarized excitation and linearly polarized excitation, the electric quadrupole and electric octupole modes are like those excited by the linearly polarized beam, only enhanced by up to a factor of 4.

These results are consistent with our previous simulation work, which showed that the "selection rules" seen here apply to a broad range of core-satellite nanostructures.[16] It was further shown that, in addition to selectively exciting and enhancing the modes, the angular scattering distribution changes with different excitation beams.

4. VARYING THE INDEX OF REFRACTION OF THE DIELECTRIC CORE

Retardation effects play an important role in the modes of the core-satellite nanostructure.[16] We investigate the role of retardation by varying the index of refraction of the dielectric core while keeping the overall size of the cluster and position of nanoparticles the same. Doing so reduces the speed of light to $c = c_0/n_{\text{core}}$ as the fields propagate through the core region , where c_0 is the speed of light in vacuum. A similar effect could be achieved by increasing the diameter of the dielectric core while keeping n_{core} fixed, since the fields would take a longer time to propagate from one end to the other. However, this would require increasing the number of particles on the surface to maintain the same density of coverage, increasing the variability in the problem. We therefor choose to vary the index of refraction, n_{core}.

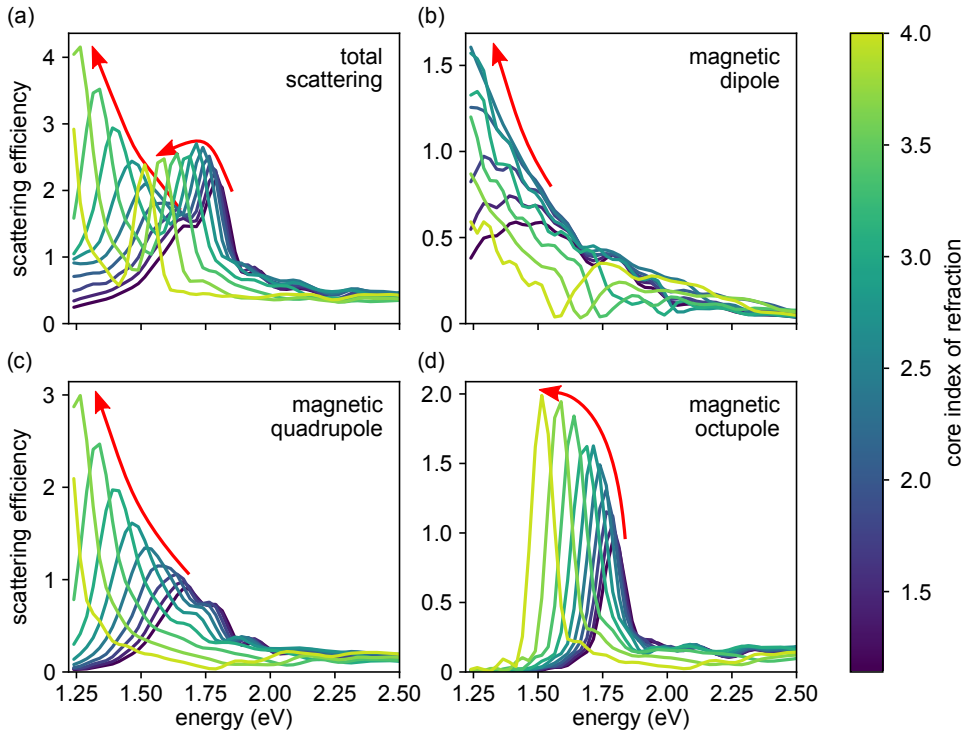

Figure 3. Total scattering and multipolar scattering are shown as a function of excitation energy and core index of refraction for azimuthally polarized beam excitation. The index of refraction of the dielectric core is varied from $n_{\text{core}} = 1$ to $n_{\text{core}} = 4$. (a) Total scattering, (b) magnetic dipole scattering, (c) magnetic quadrupole scattering, (d) magnetic octupole scattering.

Simulations are performed for 10 different core index values linearly spaced between $n_{\text{core}} = 1$ and $n_{\text{core}} = 4$ and azimuthally polarized beam excitation. The resulting total scattering spectra are shown in Figure 3(a). Curves with a brighter color correspond to higher n_{core}, and the red arrows show the trends of the scattering

modes as n_{core} increases. For $n_{\text{core}} = 1$, we observe two peaks, one at a lower energy 1.65 eV and one at a higher energy 1.8 eV. Both peaks shift to lower energies with increasing n_{core}, The lower initial energy peak is enhanced as it red-shifts, while the higher initial energy peak mostly maintains its amplitude.

A multipolar analysis is performed and in Figure 3(b-d) the scattering from magnetic dipole, magnetic quadrupole, and magnetic octupole modes are shown, respectively. This reveals the lower energy peak to be a combination of magnetic dipole and magnetic quadrupole modes while the higher energy peak is primarily a magnetic octupole mode.

The multipolar analysis reveals an interesting feature of the magnetic dipole mode that is not observable in the total scattering spectra. For core-satellite nanostructures with a high index core ($n_{\text{core}} > 3$), there are certain energy values at which the magnetic dipole vanishes entirely (Figure 3(b), from 1.5 eV to 2 eV). This energy of the vanishing point can be seen to red-shift as n_{core} is further increased. This vanishing of the magnetic dipole mode can be understood as an effect of the retardation we have introduced into the nanostructure. The azimuthally polarized beam will excite a circulation of displacement current on one side of the nanostructure at an appropriate frequency so that at a distance exactly $\lambda/2$ further, the beam will have π phase shifted and excite a circulation of displacement current on the other side of the nanostructure going the opposite way. This effectively gives us two magnetic dipoles oriented in opposite directions, so that the sum of the two is zero. Although the magnetic dipole vanishes, the remaining currents represent quadrupole or octupole-like modes.

5. AG-CORE SILICA-SHELL AG-SATELLITE NANOSTRUCTURES

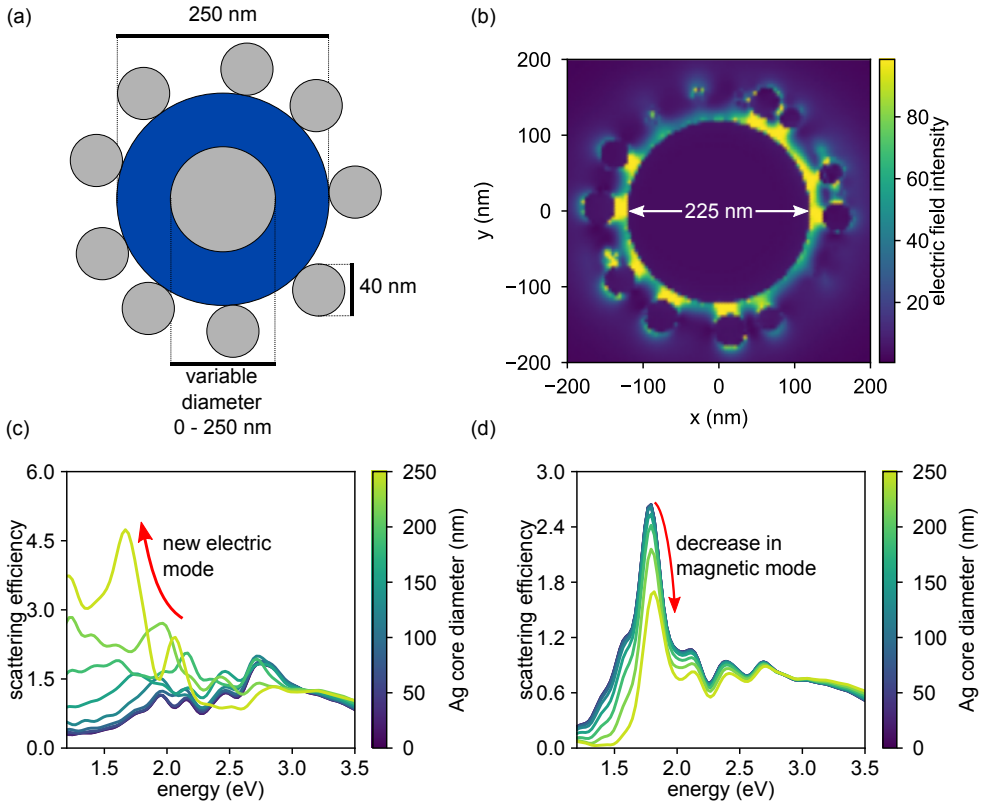

Figure 4. Ag-Core silica-shell Ag-satellite system and spectral response. A silver nanoparticle of variable diameter is surrounded by a silica shell, with 40 nm Ag nanoparticles decorating the shell to construct a core-shell-satellite structure. (a) Diagram of the core-shell-satellite structure. (b) Electric field intensity in an xy-slice of the structure under radially polarized beam excitation. (c) Scattering efficiency by radially polarized beam as a function of the nanoparticle core diameter. For a large Ag core, a new electric mode emerges. (d) Scattering efficiency by an azimuthally polarized beam as a function of the nanoparticle core diameter. The collective magnetic mode at 1.8 eV reduces in intensity with larger Ag core sizes.

The core-satellite nanostructure is (by design) strongly optically magnetic, i.e. the optical magnetic modes are much stronger than the electric modes under linearly polarized excitation (Figure 2(b)). For this reason, linearly and azimuthally polarized excitations are of particular interest to the core-satellite nanostructure owing to their collective magnetic character. The radially polarized beam, by contrast, selectively excites the weaker optical electric modes of the core-satellite nanostructure. To enhance the electric nature of the core-satellite nanostructure, we propose a new structure that we show exhibits a collective electric mode selectively excited by radially polarized light. This structure is a small modification to the core-satellite structure, and is obtained by embedding a Ag sphere in the center of the dielectric sphere, creating a core-shell-satellite structure. A diagram of this structure is shown in Figure 4(a).

We consider a Ag core diameter between 0 nm to 250 nm under radially and azimuthally polarized light. The total scattering spectra for various Ag core diameters are shown for radially polarized beam excitation in Figure 4(c) and azimuthally polarized beam excitation in Figure 4(d). For radially polarized light, a new mode appears near 1.7 eV for Ag core diameters greater than 200 nm. The new electric mode under radially polarized light is visualized in a slice of the core-shell-satellite structure with core diamter 225 nm in Figure 4(b). The radial polarization of the light is seen to strongly excite the gap region between each Ag nanoparticle and the large Ag core.

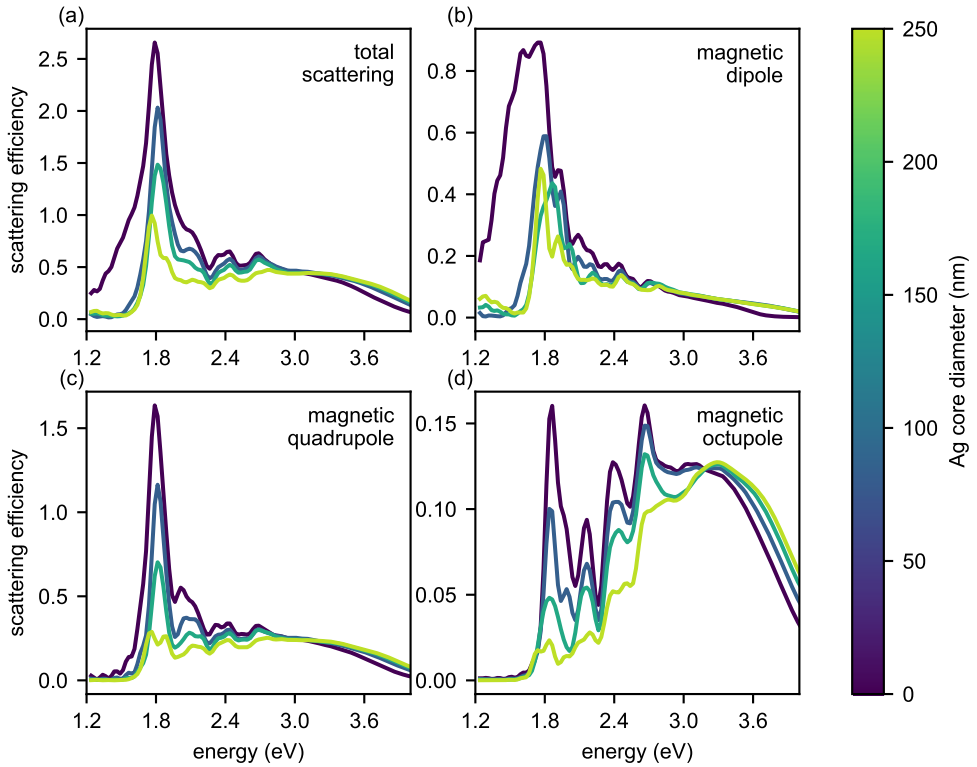

Figure 5. Scattering spectra of core-shell-satellite nanostructures. The Ag core diameter is varied between $D = 0$ nm and $D = 250$ nm in the core-shell-satellite nanostructure. Scattering and multipolar scattering are shown as a function of energy and Ag core diameter for azimuthally polarized beam excitation. (a) Total scattering, (b) magnetic dipole scattering, (c) magnetic quadrupole scattering, (d) magnetic octupole scattering.

For azimuthally polarized light, no new modes appear and instead a decrease in the 1.7 eV magnetic modes is observed with increasing Ag core diameter. We can understand this diminishing of the magnetic mode as an expulsion of the magnetic field from the core region caused by the presence of the Ag core. A circulation of

displacement currents around the perimeter of the core-satellite must generate a magnetic field in the core, as required by Faraday's Law.[15] Since the Ag core expels this magnetic field, it must also diminish the circulation of displacement currents around the perimeter. This would then diminish the magnetic modes of the nanostructure.

This diminishing effect is further demonstrated by performing a multipolar analysis of the variable core-shell-satellite nanostructure under azimuthally polarized beam excitation. The total scattering is repeated in Figure 5(a), and the multipolar scattering contributions are shown in Figure 5(b-d), for magnetic dipole, magnetic quadrupole, and magnetic octupole modes, respectively. We find that all three magnetic modes are diminished around 1.8 eV with increasing Ag core diameter. Interestingly, the magnetic quadrupole and magnetic octupole modes are diminished more effectively than the magnetic dipole mode, which is reduced by less than a factor of 2. The effect of the Ag core is much smaller at excitation energies greater than 2.4 eV, primarily affecting the magnetic octupole mode.

We conclude that although the presence of an Ag core (even of the full diameter 250 nm) diminishes the collective magnetic mode of the nanostructure, some amount of magnetic field persists and is mostly due to a surviving magnetic dipole mode.

6. CONCLUSIONS

We have utilized a method of multipolar analysis in FDTD simulations and applied it to understand the interaction of vector beams with SiO_2-Ag core-satellite nanostructures. This method can be used to identify the multipolar nature of scattering peaks and provide a way to better understand and control the modes of the core-satellite nanostructure. The cylindrical vector beams are shown to selectively excite certain modes of the core-satellite nanostructure at optical frequencies, making them a powerful spectroscopic technique for uniquely identifying novel optical modes of nanoscale structures.

Retardation effects are demonstrated by varying the index of refraction of the core region. Combined with the multipolar analysis, a characterization of the shifting modes was made possible. A unique effect was observed with high index cores where the magnetic dipole mode vanishes due to two out-of-phase magnetic dipole excitations. This detailed analysis can help guide the construction and optimization of new core-satellite nanostructures for us in meta-materials and meta-fluids.

While the core-satellite structure exhibits magnetic modes visible frequencies, we examined a new core-shell-satellite structure that allows a new enhanced collective electric mode. Nanostructures with a unique radial character like these structures can be used to further study the interaction of the radially polarized beam with nanoscale structures. These unique collective modes can be selectively excited and enhanced with the vector beam sources, leading to new spectroscopic techniques to identify these modes.

ACKNOWLEDGMENTS

The authors acknowledge support from the Vannevar Bush Faculty Fellowship program sponsored by the Basic Research Office of the Assistant Secretary of Defense for Research and Engineering and funded by the Office of Naval Research (N00014-16-1-2502). This work was performed, in part, at the Center for Nanoscale Materials, a U.S. Department of Energy Office of Science User Facility, and supported by the U.S. Department of Energy, Office of Science, under Contract No. DE-AC02-06CH11357. We also acknowledge the University of Chicago Research Computing Center for providing the computational resources needed for this work.

REFERENCES

[1] Veselago, V. G., "The electrodynamics of substances with simultaneously negative values of ϵ and μ," *Soviet Physics Uspekhi* **10**(4), 509 (1968).

[2] Smith, D. R., Pendry, J. B., and Wiltshire, M., "Metamaterials and negative refractive index," *Science* **305**(5685), 788–792 (2004).

[3] Bourgeois, M. R., Liu, A. T., Ross, M. B., Berlin, J. M., and Schatz, G. C., "Self-assembled plasmonic metamolecules exhibiting tunable magnetic response at optical frequencies," *The Journal of Physical Chemistry C* **121**(29), 15915–15921 (2017).

[4] Fan, J. A., Wu, C., Bao, K., Bao, J., Bardhan, R., Halas, N. J., Manoharan, V. N., Nordlander, P., Shvets, G., and Capasso, F., "Self-assembled plasmonic nanoparticle clusters," *Science* **328**(5982), 1135–1138 (2010).

[5] Alù, A., Salandrino, A., and Engheta, N., "Negative effective permeability and left-handed materials at optical frequencies," *Optics Express* **14**(4), 1557–1567 (2006).

[6] Sheikholeslami, S. N., Alaeian, H., Koh, A. L., and Dionne, J. A., "A metafluid exhibiting strong optical magnetism," *Nano Letters* **13**(9), 4137–4141 (2013).

[7] Fruhnert, M., Mühlig, S., Lederer, F., and Rockstuhl, C., "Towards negative index self-assembled metamaterials," *Physical Review B* .

[8] Qian, Z., Hastings, S. P., Li, C., Edward, B., McGinn, C. K., Engheta, N., Fakhraai, Z., and Park, S., "Raspberry-like metamolecules exhibiting strong magnetic resonances," *ACS Nano* **9**(2), 1263–1270 (2015).

[9] Vallecchi, A., Albani, M., and Capolino, F., "Collective electric and magnetic plasmonic resonances in spherical nanoclusters," *Optics Express* **19**(3), 2754–2772 (2011).

[10] Mühlig, S., Cunningham, A., Scheeler, S., Pacholski, C., Bürgi, T., Rockstuhl, C., and Lederer, F., "Self-assembled plasmonic core–shell clusters with an isotropic magnetic dipole response in the visible range," *ACS Nano* **5**(8), 6586–6592 (2011).

[11] Ponsinet, V., Barois, P., Gali, S. M., Richetti, P., Salmon, J., Vallecchi, A., Albani, M., Le Beulze, A., Gomez-Grana, S., Duguet, E., Mornet, S., and Treguer-Delapierre, M., "Resonant isotropic optical magnetism of plasmonic nanoclusters in visible light," *Physical Review B* **92**(22), 220414 (2015).

[12] Gandra, N., Abbas, A., Tian, L., and Singamaneni, S., "Plasmonic planet–satellite analogues: hierarchical self-assembly of gold nanostructures," *Nano Letters* **12**(5), 2645–2651 (2012).

[13] Das, T., Iyer, P. P., DeCrescent, R. A., and Schuller, J. A., "Beam engineering for selective and enhanced coupling to multipolar resonances," *Physical Review B* **92**(24), 241110 (2015).

[14] Woźniak, P., Banzer, P., and Leuchs, G., "Selective switching of individual multipole resonances in single dielectric nanoparticles," *Laser & Photonics Reviews* **9**(2), 231–240 (2015).

[15] Manna, U., Lee, J.-H., Deng, T.-S., Parker, J., Shepherd, N., Weizmann, Y., and Scherer, N. F., "Selective induction of optical magnetism," *Nano Letters* **17**(12), 7196–7206 (2017).

[16] Parker, J., Gray, S., and Scherer, N., "Multipolar analysis of electric and magnetic modes excited by vector beams in core-satellite nano-structures," *arxiv:1711.06833* (2017).

[17] Taflove, A. and Hagness, S. C., "Computational electrodynamics: the finite-difference time-domain method," *Norwood, 2nd Edition, MA: Artech House* (1995).

[18] Ardavan, F. O., David, R., Mihai, I., Peter, B., Joannopoulos, J. D., and Steven, G. J., "MEEP: A flexible free-software package for electromagnetic simulations by the FDTD method," *Computer Physics Communications* **181**, 687–702 (January 2010).

[19] Johnson, P. B. and Christy, R. W., "Optical constants of the noble metals," *Physical Review B* **6**(12), 4370 (1972).

[20] Rakić, A. D., Djurišić, A. B., Elazar, J. M., and Majewski, M. L., "Optical properties of metallic films for vertical-cavity optoelectronic devices," *Applied Optics* **37**(22), 5271–5283 (1998).

[21] Farjadpour, A., Roundy, D., Rodriguez, A., Ibanescu, M., Bermel, P., Joannopoulos, J. D., Johnson, S. G., and Burr, G., "Improving accuracy by subpixel smoothing in FDTD," *Optics Letters* **31**, 2972–2974 (October 2006).

[22] Oskooi, A. F., Kottke, C., and Johnson, S. G., "Accurate finite-difference time-domain simulation of anisotropic media by subpixel smoothing," *Optics Letters* **34**, 2778–2780 (September 2009).

[23] Zhan, Q., "Cylindrical vector beams: from mathematical concepts to applications," *Advances in Optics and Photonics* **1**(1), 1–57 (2009).

[24] Novotny, L. and Hecht, B., "Principles of nano-optics," *Cambridge University Press* (2012).

[25] Ramahi, O. M., "Near-and far-field calculations in fdtd simulations using kirchhoff surface integral representation," *IEEE Transactions on Antennas and Propagation* **45**(5), 753–759 (1997).

[26] Mühlig, S., Menzel, C., Rockstuhl, C., and Lederer, F., "Multipole analysis of meta-atoms," *Metamaterials* **5**(2), 64–73 (2011).

[27] Grahn, P., Shevchenko, A., and Kaivola, M., "Electromagnetic multipole theory for optical nanomaterials," *New Journal of Physics* **14**(9), 093033 (2012).